

Supplementary Material

Ligand-Driven Facet Control of InAs-Based Quantum Dots for Enhanced Near- and Shortwave Infrared Emission

*Hyunjin Cho¹, Yujin Kim¹, Whi Dong Kim^{2,3} Young-Shin Park⁴, Ju Young Woo^{*3,5,6}, Hyung-Kyu Lim^{*7}, Doh C. Lee^{*1}*

¹*Department of Chemical and Biomolecular Engineering, Energy and Environmental Research Center (EERC), KAIST Institute for NanoCentury (KINC), Korea Advanced Institute of Science and Technology (KAIST), Daejeon 34141, Republic of Korea*

²*Carbon Neutral Technology R&D Department, Korea Institute of Industrial Technology (KITECH), Cheonan 31056, Republic of Korea*

³*Autonomous Manufacturing and Process Department, KITECH, Ansan 15588, Republic of Korea*

⁴*Chemistry Division, Los Alamos National Laboratory, Los Alamos, New Mexico 87545, United States*

⁵*School of Integrative Engineering, Chung-Ang University, Seoul 06974, Republic of Korea*

⁶*HYU-KITECH Joint Department, Hanyang University, Ansan 15588, Republic of Korea*

⁷*Division of Chemical and Bioengineering, Kangwon National University, Chuncheon, 24341, Republic of Korea*

1 Supplementary Figures and Tables

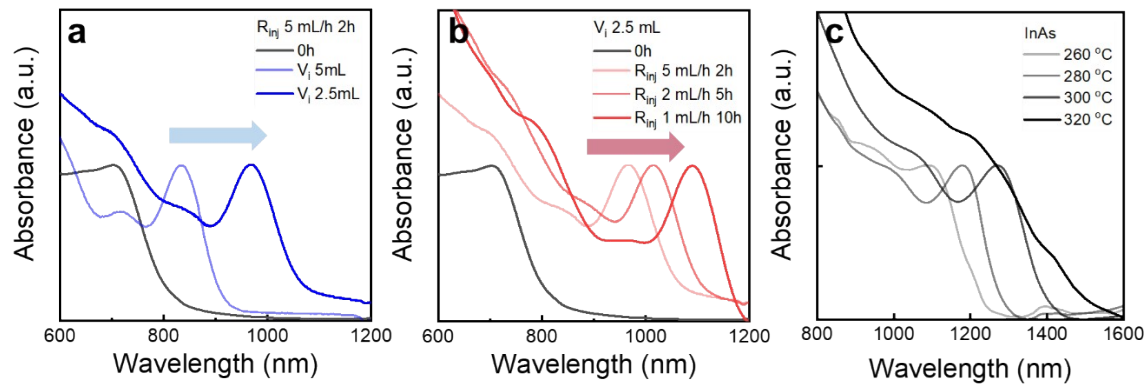
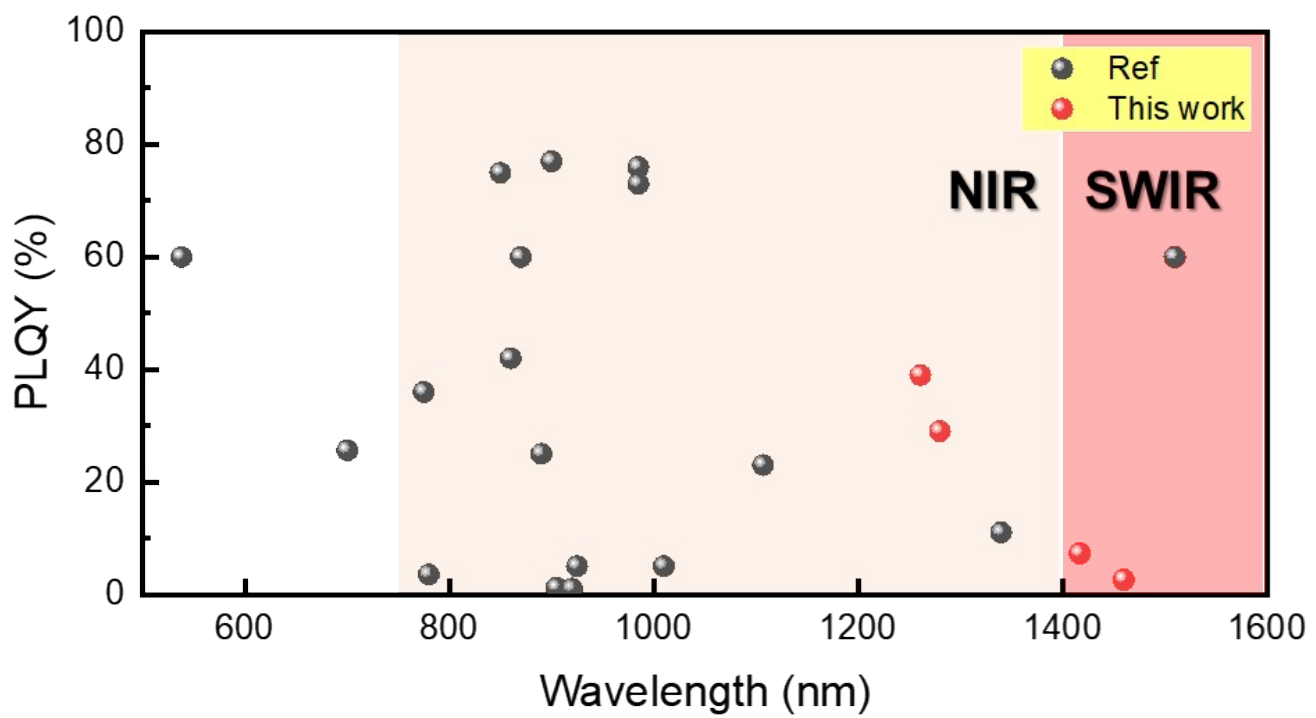


Figure S1. Absorption spectra of InAs QDs under different synthesis conditions. Absorption spectra (a) for injection rates of 5 mL/h (2 hours), with initial volumes of 5 mL and 2.5 mL. (b) for an initial volume of 2.5 mL, with injection rates of 5 mL/h (2 hours), 2 mL/h (5 hours), and 1 mL/h (10 hours). (c) at temperatures of 260°C, 280°C, 300°C, and 320°C.

Table S1. Summary of InAs-based QDs and their optical characteristics

Core material	Shell material	PL peak (nm)	FWHM (nm)	PLQY (%)	Ref
InAs	InP	N/A	N/A	N/A	1
InAs	InP	N/A	N/A	N/A	2
InAs	InP	905	60-75	1.2	3
InAs	InP/ZnSe	625-780	68	3.5	4
InAs	InP/ZnSe	985	60-75	76	3
InAs	InP/ZnSe	~870	~75	60	5
InAs	InP/ZnSe/ZnS	~775	~150	36	6
InAs	InZnP/GaP/ZnSe	~1107	~124	23	7
InAs	In(Zn)P/ZnSe/ZnS	~890	~90	25	8
InAs	ZnSe	1300	110-180	N/A	9
InAs	ZnSe	750-920	85-121	1-2	10
InAs	ZnSe	1010	147	5-10	11
InAs	ZnS	925	111	5-10	11
In(Zn)As	ZnSe/ZnS	538	60	60	12
In(Zn)As	In(Zn)P/GaP/ZnS	~850	110	75	13 and 14
InGa _{0.2} As _{0.8}	ZnSe	580-700	~50	25.6	15
Zn-InAs	ZnSe	860	195	42	16
InAs	ZnSe	900	134	77	17
In(Zn)As	In(Zn)P/GaP/ZnS	985	124	73	18
InAs	ZnSe/ZnS	1340	147	11	19
InAs(rod)	ZnSe	1510	180	60	20

InAs	In(Zn)P/ZnSe/ZnS	~1500	147	39 @1260nm	This study
------	------------------	-------	-----	------------	-------------------



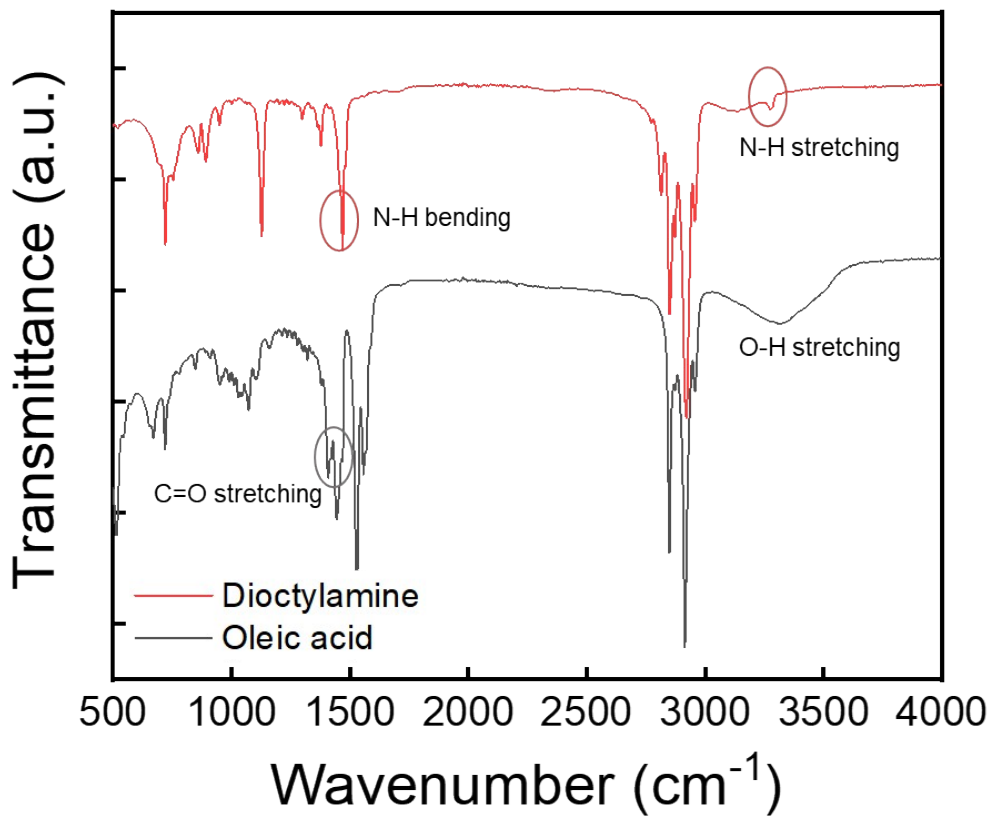


Figure S2. Fourier transform infrared (FTIR) spectra of InAs core QDs with dioctylamine and oleic acid as ligands.

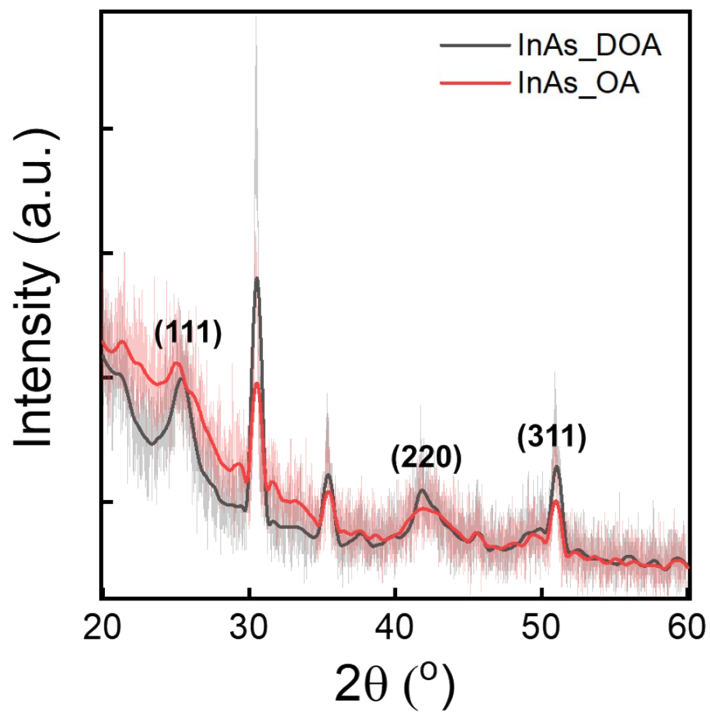


Figure S3. X-ray diffraction (XRD) patterns of InAs QDs synthesized with different ligands.

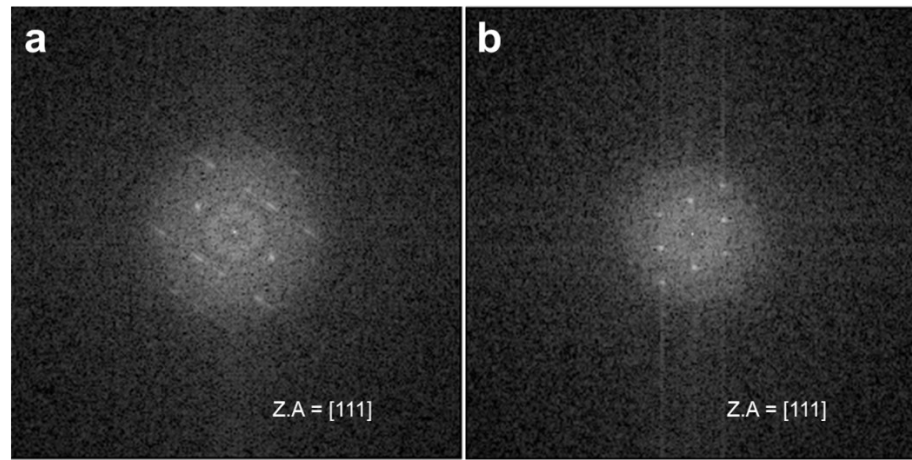


Figure S4. Fast fourier transform (FFT) of InAs QDs using a) dioctylamine and b) oleic acid as ligands.

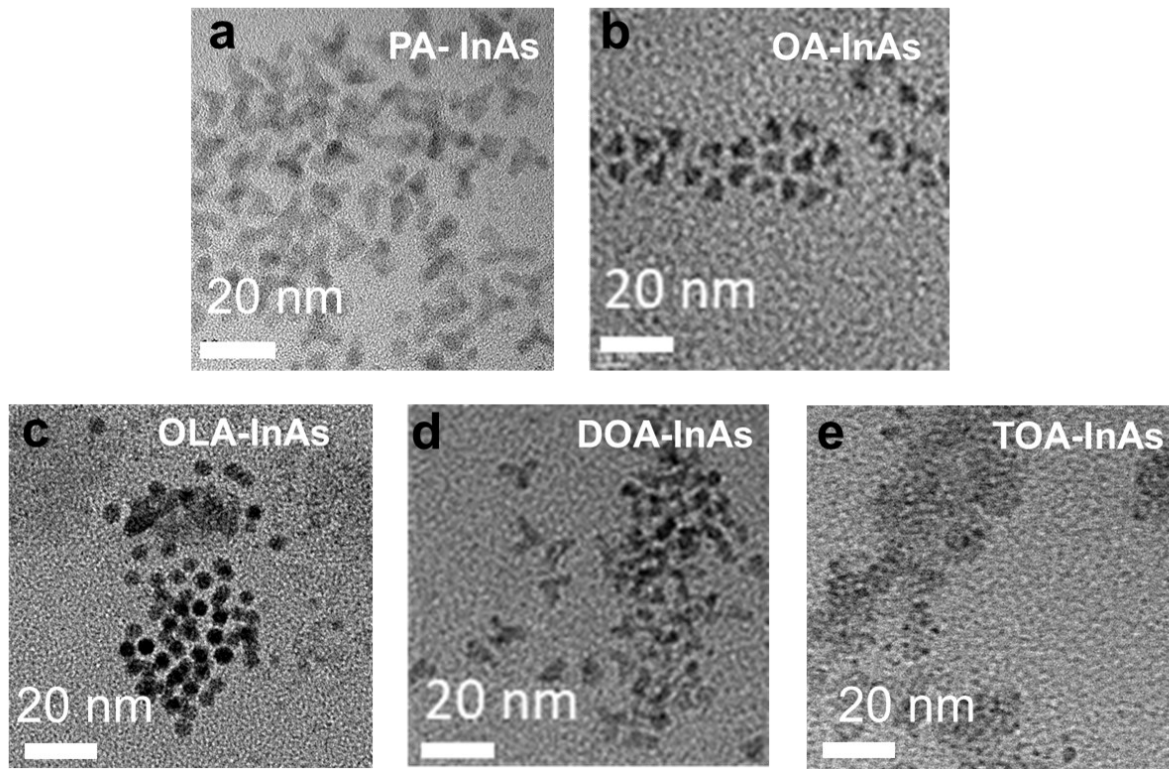


Figure S5. Transmission electron microscopy (TEM) images of InAs QDs synthesized with different ligands, showing the 1S peak at approximately 1300 nm. (a) PA-InAs: palmitic acid (PA), (b) OA-InAs: oleic acid (OA), (c) OLA-InAs: oleylamine (OLA), (d) DOA-InAs: dioctylamine (DOA), (e) TOA-InAs: trioctylamine (TOA).

Table S2. Surface energy and dipole of InAs QDs based on facets

Surface	Γ (eV/Å ²)	Surface Dipole (eÅ/Å ²)
(111)	0.101	0.013
(110)	0.057	0.000

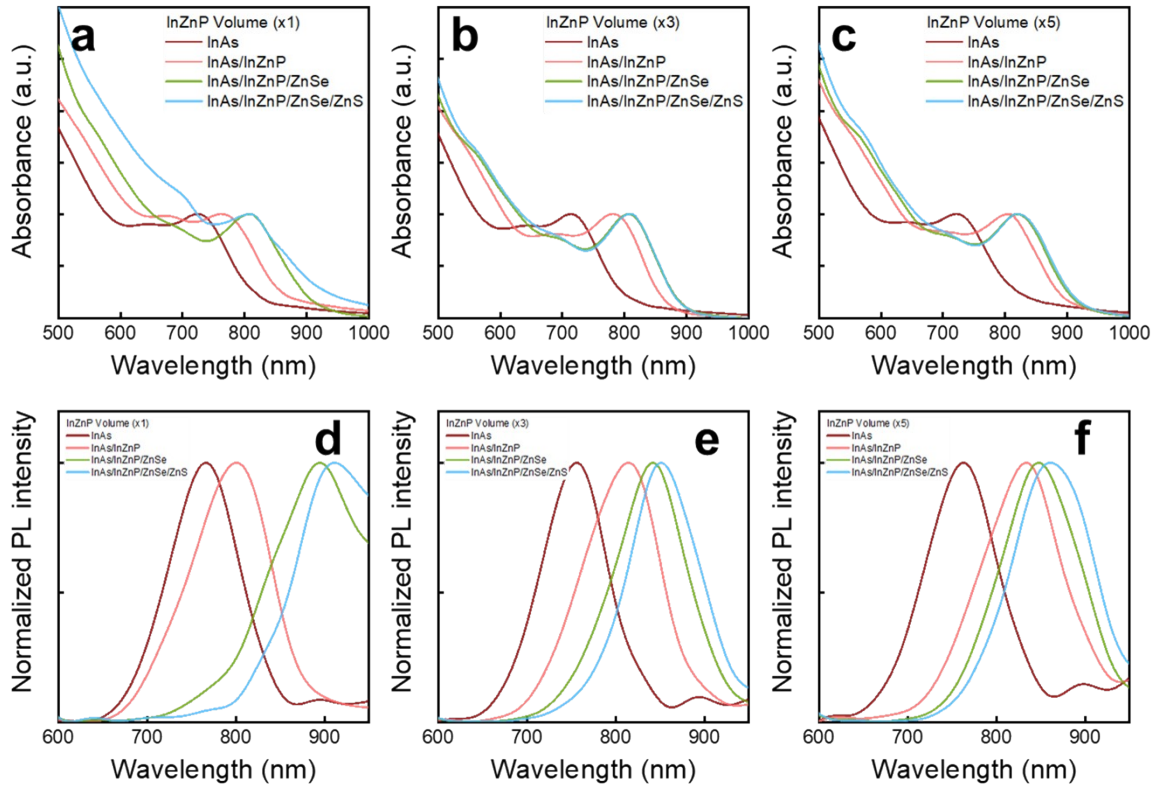


Figure S6. Absorption Spectra and PL spectra of InAs/InZnP/ZnSe/ZnS Structures. Absorption spectra with InZnP volume a) x1, b) x3, c) x5. PL spectra with InZnP volume d) x1, e) x3, f) x5.

Table S3. Photoluminescence quantum yield (PLQY) of InAs/InZnP/ZnSe/ZnS QDs

PLQY(%) /InZnP Volume	InAs	InAs/InZnP	InAs/InZnP/ZnSe	InAs/InZnP/ZnSe/ZnS
x1	1.2	3.4	4.3	5.2
x3	1.3	5.8	29.4	35.3
x5	1	6.1	29	40.9

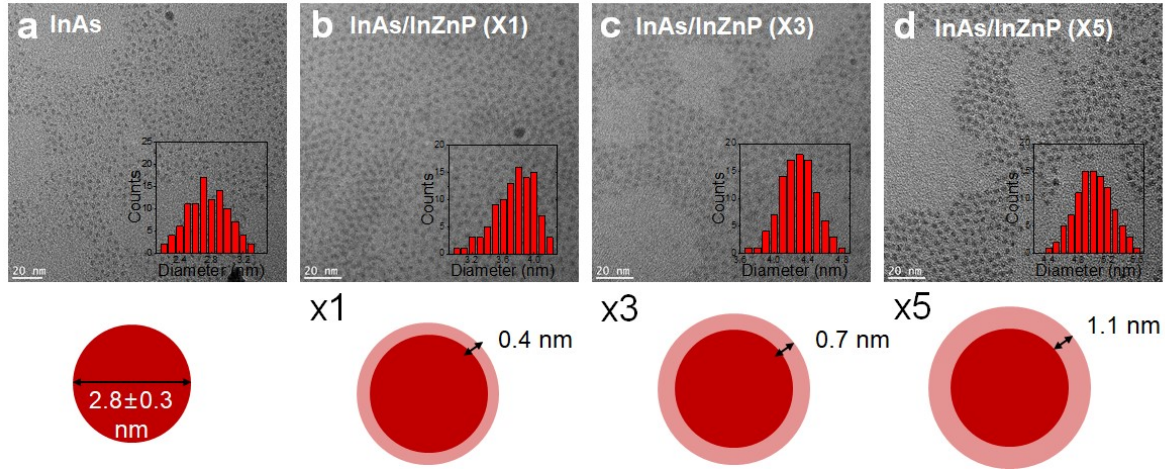


Figure S7. TEM images and schematic representations of InAs QDs with different InZnP shell volumes. (a) TEM image of InAs QDs with a size distribution of 2.80 ± 0.30 nm. (b, c, d) TEM images of InAs/InZnP QDs with an InZnP volume of x1 (3.66 ± 0.26 nm), x3 (4.28 ± 0.21 nm), and x5 (5.00 ± 0.25 nm) relative to the InAs nanocluster volume, respectively.

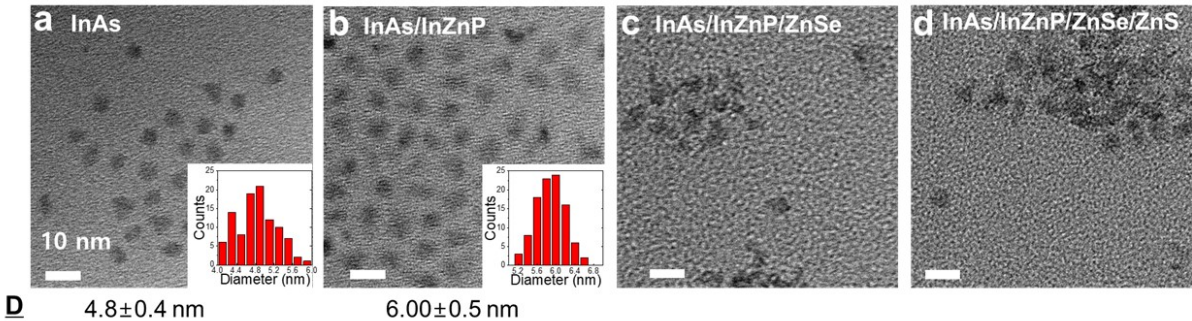


Figure S8. TEM images of InAs QDs showing the 1S peak at approximately 1100 nm and their core-shell structures with different shells. (a) TEM image of InAs QDs, inset: size distribution 4.83 ± 0.41 nm. (b) TEM image of InAs/InZnP core-shell QDs, inset: 5.88 ± 0.31 nm. (c) TEM image of InAs/InZnP/ZnSe core-multi-shell QDs. (d) TEM image of InAs/InZnP/ZnSe/ZnS core-multi-shell QDs.

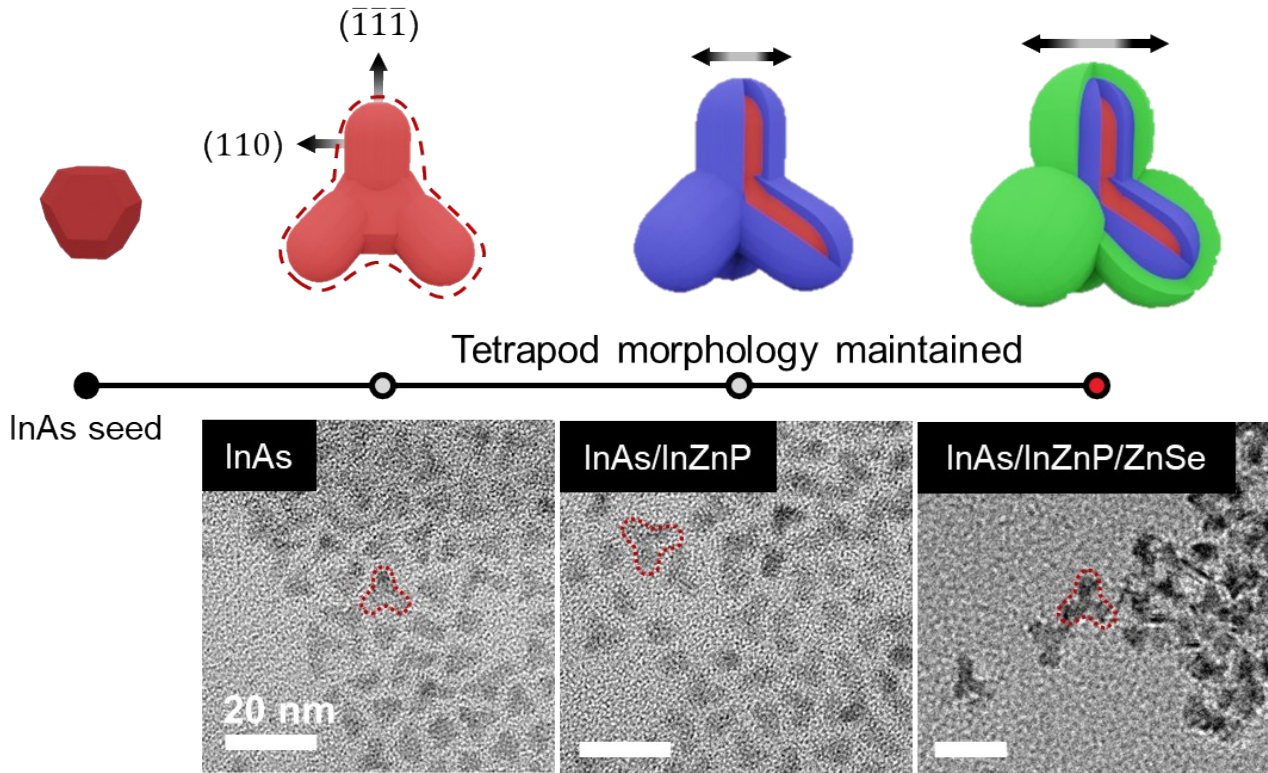


Figure S9. Scheme and TEM images for InZnP and ZnSe shell growth on InAs core using dioctylamine as ligand with 1S peak at approximately 1250 nm. As the seed growth continues, arms develop on the $(\bar{1}\bar{1}1)$ facets forming a tetrapod morphology. This morphology is maintained throughout the shelling process, with a slight increase in arm width. The average width of InAs and InAs/InZnP is 3.29 ± 0.33 nm and 4.58 ± 0.65 nm, respectively.

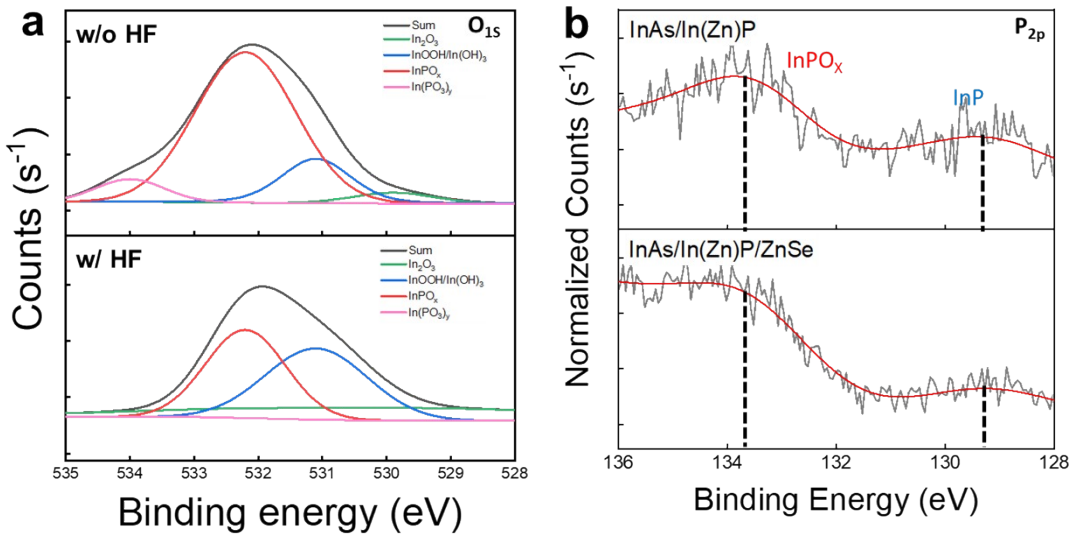


Figure S10. a) X-ray Photoelectron Spectroscopy (XPS) spectrum of O 1s for InAs/InZnP/ZnSe QDs with and without HF treatment. b) XPS spectrum of P 2p for InAs/InZnP QDs and InAs/InZnP/ZnSe QDs without HF treatment.

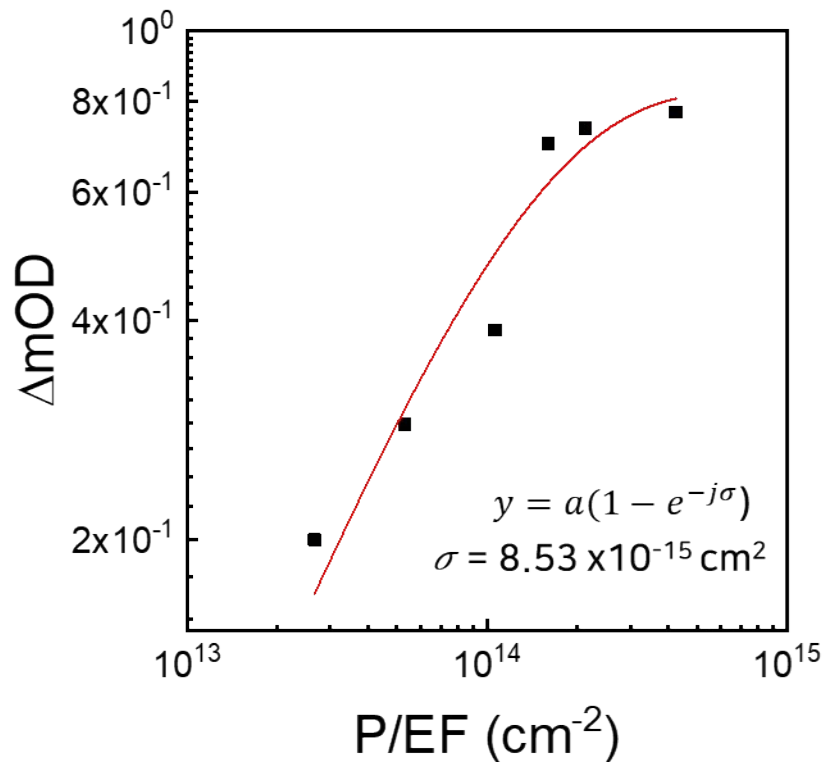


Figure S11. At lower levels of laser pumping, the saturation curves of transient absorption spectroscopy for InAs/InZnP/ZnSe/ZnS QDs with dioctylamine are modeled by Counts $\propto 1 - e^{-\langle N \rangle} = 1 - e^{-j\sigma}$, where j represents the laser pump fluence and σ denotes the absorption cross-section. Here, j is calculated as P/EF , with P being the laser power density, E the laser repetition rate (200 kHz), and F the photon energy at 700 nm. This establishes the theoretical function $\langle N \rangle = j\sigma = \sigma P/EF$, showing a linear relationship between $\langle N \rangle$ and P , determined by the factor σ/EF .

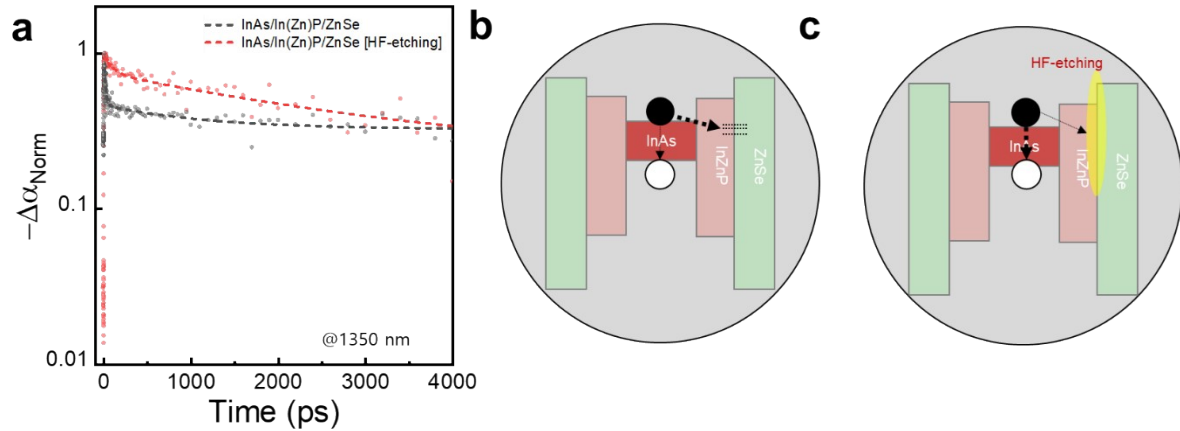


Figure S12. Transient absorption spectroscopy and schematic representation of InAs/InZnP/ZnSe QDs using dioctylamine as a ligand before and after HF treatment. (a) Ground state bleaching (GSB) decay curves from transient absorption spectroscopy for InAs/InZnP/ZnSe QDs before (black) and after (red) HF treatment. (b-c) Schematic representation of the InAs/InZnP/ZnSe QDs before and after HF treatment, showing the core-shell structure and the positions of electrons (e^-) and holes (h^+) within the QDs.

Table S4. The decay constants (A_1 , τ_1 , A_2 , τ_2) for the GSB observed in the transient absorption spectroscopy, comparing the values before and after HF treatment

	InAs/InZnP/ZnSe	InAs/InZnP/ZnSe [HF-etching]
A_1	0.73	0.28
τ_1 (ps)	19.41 ± 3.10	101.59 ± 28.30
A_2	0.27	0.72
τ_2 (ps)	1108.03 ± 629.69	2776.46 ± 983.87

Table S5: Optical properties of InAs QDs with different core/shell structures: InAs, InAs/InZnP, InAs/InZnP/HF, InAs/InZnP/HF/ZnSe, and InAs/InZnP/HF/ZnSe/ZnS

	InAs	InAs/InZnP	InAs/InZnP (HF)	InAs/InZnP(HF)/ZnSe	InAs/InZnP(HF)/ZnSe/ZnS
Emission wavelength (nm)	727.2	812.2	826.8	832.7	837.8
FWHM (nm)	73.3	96.3	97.8	105.6	102.7
PLQY (%)	4.7	7.7	10.5	20.1	42.9

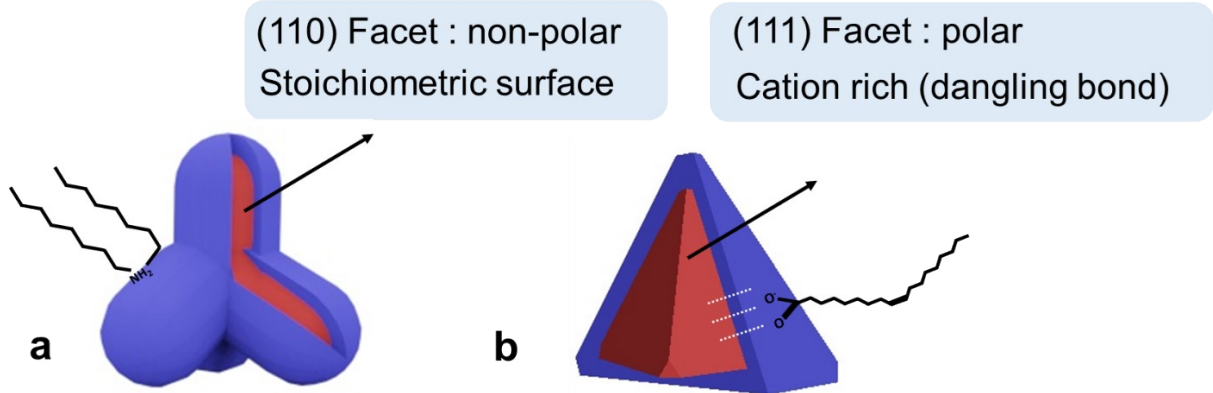


Figure S13. Schematic representations of InAs-based QDs with different facets. Illustration of InAs-based QDs (a) with (110) non-polar facets, showing stoichiometric surfaces and (b) with (111) polar facets, showing cation-rich surfaces with dangling bonds.

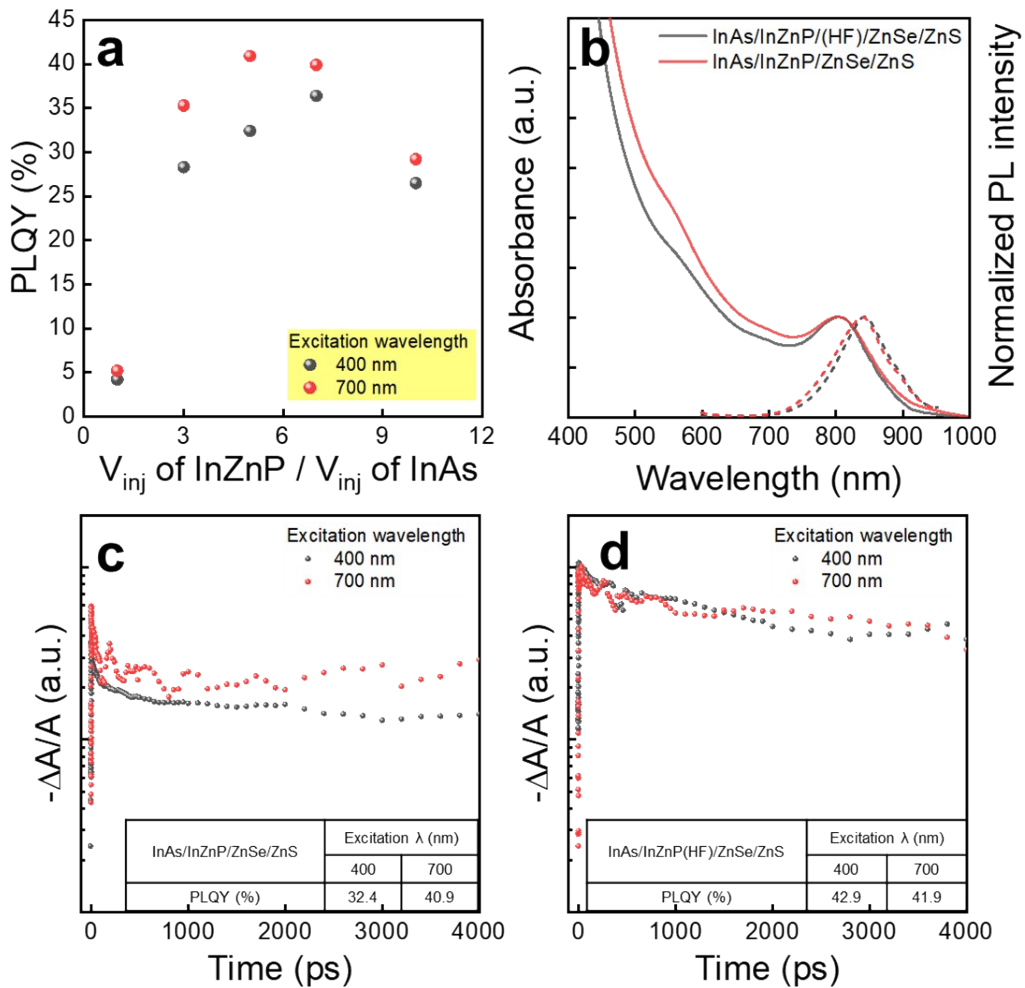


Figure S14. Optical and exciton dynamic properties of InAs/InZnP/ZnSe/ZnS QDs using dioctylamine as a ligand with an emission peak at 850 nm. (a) PLQY differences at excitation wavelengths of 400 nm and 700 nm for InAs/InZnP/ZnSe/ZnS QDs. (b) Absorption and PL spectra of InAs/InZnP/ZnSe/ZnS QDs before (red) and after (black) HF treatment. (c-d) Transient absorption GSB decay of InAs/InZnP/ZnSe/ZnS QDs: (c) before and (d) after HF treatment at excitation wavelengths of 400 nm (shell) and 700 nm (core). The inset shows the PLQY of QDs with different excitation wavelengths.

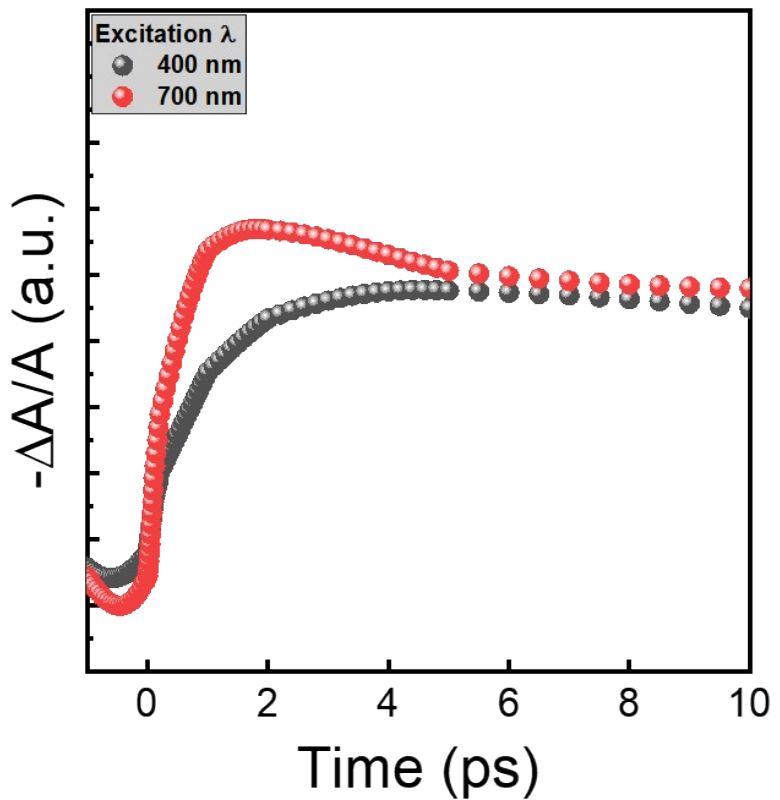


Figure S15. Transient absorption spectroscopy of GSB decay curves for InAs core QDs upon excitation at 400 nm and 700 nm, respectively.

Table S6. Decay dynamics in GSB of InAs/InZnP/ZnSe/ZnS QDs with dioctylamine and oleic acid ligands at 400 nm and 700 nm excitation wavelengths

	Dioctylamine		Oleic acid	
	λ_{ex}		λ_{ex}	
	400 nm	700 nm	400 nm	700 nm
A ₁ (%)	25	67	5	35
τ_1 (ps)	160	154	52	54
A ₂ (%)	75	33	95	65
τ_2 (ps)	17400	17400	14400	14400

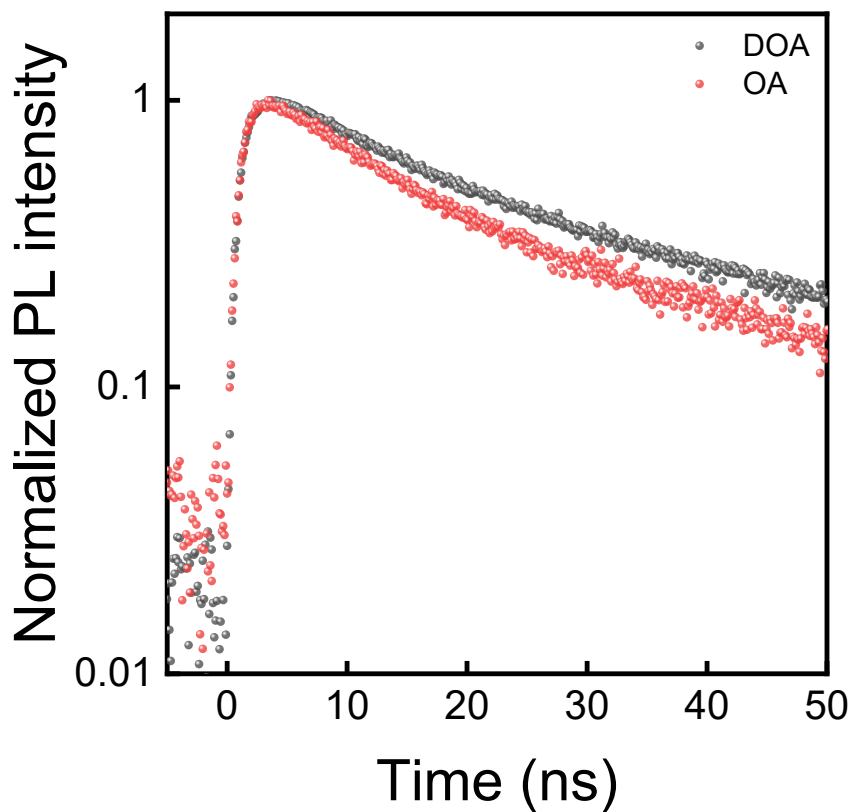


Figure S16. Time-resolved photoluminescence (TRPL) data for NIR InAs/InZnP/ZnSe/ZnS QDs with different ligands (dioctylamine and oleic acid) recorded using a nanosecond pulsed laser with 950 nm excitation. The emission decay was monitored at 1260 nm.

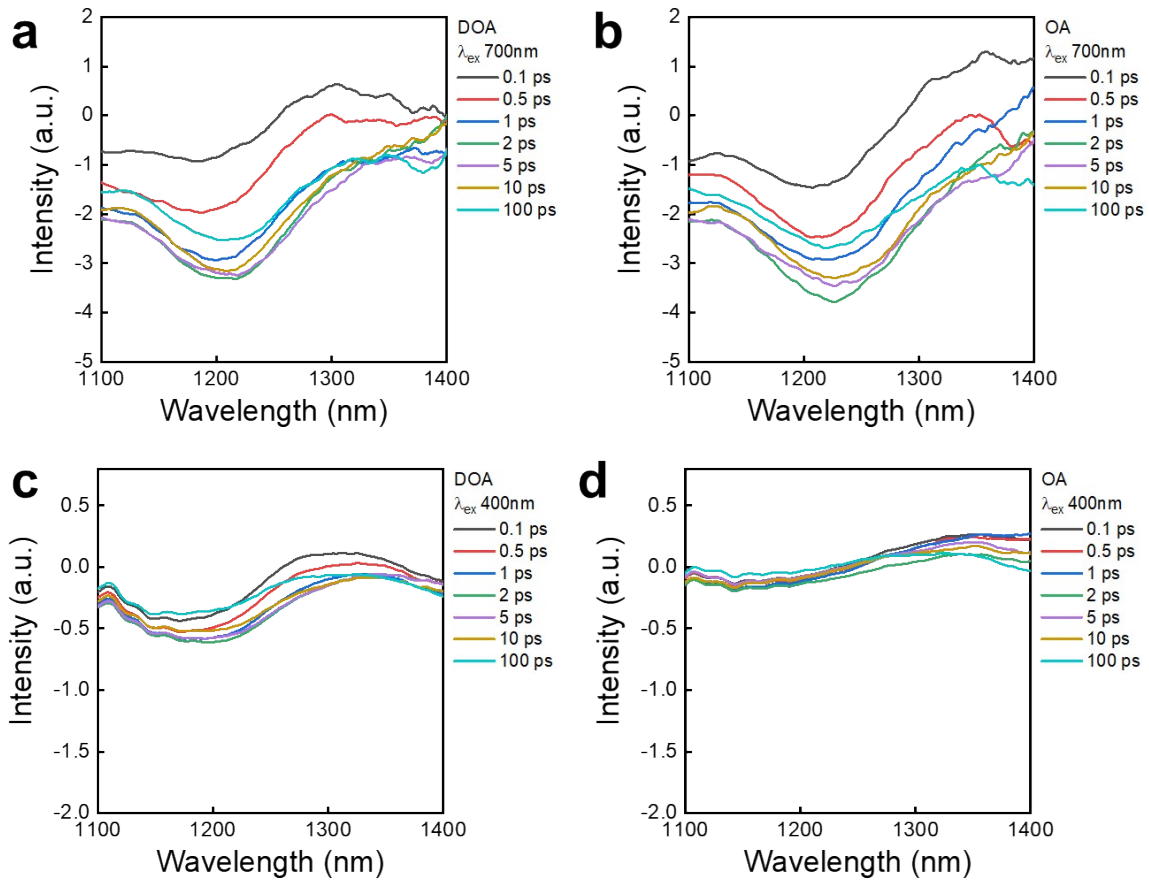


Figure S17. Transient absorption spectroscopy data for InAs/InZnP/ZnSe/ZnS QDs in the NIR region. a) and b) show data for QDs using dioctylamine (DOA) and oleic acid (OA) as ligands, respectively, excited at a wavelength of 700 nm $\langle N \sim 0.1 \rangle$. c) and d) present data for QDs using DOA and OA ligands, respectively, excited at a wavelength of 400 nm $\langle N \sim 0.1 \rangle$. All intensity values are normalized by the corresponding absorption. Measurements were taken at various time points: 0.1 ps, 0.5 ps, 1 ps, 2 ps, 5 ps, 10 ps, and 100 ps.

References

1. Y. Cao and U. Banin, Growth and properties of semiconductor core/shell nanocrystals with InAs cores. *J. Am. Chem. Soc.*, **2000**, 122, 9692–9702.
2. Y. W. Cao and U. Banin, Synthesis and characterization of InAs/InP and InAs/CdSe core/shell nanocrystals. *Angew. Chem., Int. Ed.*, **1999**, 38, 3692–3694.
3. R. Xie, K. Chen, X. Chen and X. Peng, InAs/InP/ZnSe core/shell/shell quantum dots as near-infrared emitters: Bright, narrow-band, non-cadmium containing, and biocompatible. *Nano Res.*, **2008**, 1, 457–464.
4. S.-W. Kim, J. P. Zimmer, S. Ohnishi, J. B. Tracy, J. V. Frangioni and M. G. Bawendi, Engineering InAs_xP_{1-x}/InP/ZnSe III–V Alloyed Core/Shell Quantum Dots for the Near-Infrared. *J. Am. Chem. Soc.*, **2005**, 127, 10526–10532.
5. M. J. Enright, D. Jasrasaria, M. M. Hanchard, D. R. Needell, M. E. Phelan, D. Weinberg, B. E. McDowell, H.-W. Hsiao, H. Akbari and M. Kottwitz, Role of atomic structure on exciton dynamics and photoluminescence in NIR emissive InAs/InP/ZnSe quantum dots. *J. Phys. Chem. C*, **2022**, 126, 7576–7587.
6. J. Zhang, R. Li, W. Sun, Q. Wang, X. Miao and D. Zhang, Temporal evolutions of the photoluminescence quantum yields of colloidal InP, InAs and their core/shell nanocrystals. *J. Mater. Chem. C*, **2014**, 2, 4442–4448.
7. L. K. Sagar, G. Bappi, A. Johnston, B. Chen, P. Todorovic', L. Levina, M. I. Saidaminov, F. P. Garcí'a de Arquer, S. Hoogland and E. H. Sargent, Single-precursor intermediate shelling enables bright, narrow line width InAs/InZnP-based QD emitters. *Chem. Mater.*, **2020**, 32, 2919–2925.
8. H. Wijaya, D. Darwan, K. R. G. Lim, T. Wang, K. H. Khoo and Z.-K. Tan, Large-strokes-shifted infrared-emitting InAs–In (Zn) P–ZnSe–ZnS giant-shell quantum dots by one-pot continuous-injection synthesis. *Chem. Mater.*, **2019**, 31, 2019–2026.
9. N. Tessler, V. Medvedev, M. Kazes, S. Kan, and U. Banin, Efficient near-infrared polymer nanocrystal light-emitting diodes. *Science*, **2002**, 295, 1506–1508.
10. J. P. Zimmer, S.-W. Kim, S. Ohnishi, E. Tanaka, J. V. Frangioni and M. G. Bawendi, Size Series of Small Indium Arsenide–Zinc Selenide Core–Shell Nanocrystals and Their Application to In Vivo Imaging. *J. Am. Chem. Soc.*, **2006**, 128, 2526–2527.
11. V. Grigel, D. Dupont, K. De Nolf, Z. Hens and M. D. Tessier, InAs colloidal quantum dots synthesis via aminopnictogen precursor chemistry. *J. Am. Chem. Soc.*, **2016**, 138, 13485–13488.
12. D. Darwan, L. J. Lim, T. Wang, H. Wijaya and Z.-K. Tan, Ultra-confined visible-light-emitting colloidal indium arsenide quantum dots. *Nano Lett.*, **2021**, 21, 5167–5172.
13. K. R. G. Lim, D. Darwan, H. Wijaya, Z. C. Lim, J. Shanmugam, T. Wang, L. J. Lim, W. H. Ang and Z. K. Tan, High Quantum Yield Water-Dispersed Near-Infrared In (Zn) As–In (Zn) P–GaP–ZnS Quantum Dots with Robust Stability for Bioimaging. *Adv. Mater. Interfaces*, **2020**, 7, 2000920.

14. H. Wijaya, D. Darwan, X. Zhao, E. W. Y. Ong, K. R. G. Lim, T. Wang, L. J. Lim, K. H. Khoo and Z. K. Tan, Efficient Near-Infrared Light-Emitting Diodes based on In (Zn) As–In (Zn) P–GaP–ZnS Quantum Dots. *Adv. Funct. Mater.*, **2020**, 30, 1906483.
15. J. P. Park, J.-j Lee and S.-W. Kim, Fabrication of GaAs, $\text{In}_x\text{Ga}_{1-x}\text{As}$ and Their ZnSe Core/Shell Colloidal Quantum Dots. *J. Am. Chem. Soc.*, **2016**, 138, 16568–16571.
16. D. Zhu, F. Bellato, H. Bahmani Jalali, F. Di Stasio, M. Prato, Y. P. Ivanov, G. Divitini, I. Infante, L. De Trizio and L. Manna, ZnCl_2 Mediated Synthesis of InAs Nanocrystals with Aminoarsine. *J. Am. Chem. Soc.*, **2022**, 144, 10515–10523.
17. H. Roshan, D. Zhu, D. Piccinotti, J. Dai, M. De Franco, M. Barelli, M. Prato, L. De Trizio, L. Manna, and F. Di Stasio, Near Infrared Light-Emitting Diodes Based on Colloidal InAs/ZnSe Core/Thick-Shell Quantum Dots. *Adv. Sci.* **2024**, 11, 2400734
18. X. Zhao, L. J. Lim, S. S. Ang, and Z.-K. Tan, Efficient short-wave infrared light-emitting diodes based on heavy-metal-free quantum dots. *Adv. Mater.* **2022**, 34, 2206409
19. X. Shan, Y. Zhou, B. Li, Z. Zeng, and B. Ji, Wurtzite InAs Nanocrystals with Short-Wavelength Infrared Emission Synthesized through the Cation Exchange of Cu_3As Nanocrystals. *Chem. Mater.* **2023**, 35, 2569–2578
20. T. Sheikh, W. J. Mir, A. Alofi, M. Skoroterski, R. Zhou, S. Nematulloev, M. N. Hedhili, M. B. Hassine, M. S. Khan, K. E. Yorov, B. E. Hasanov, H. Liao, Y. Yang, A. Shamim, M. Abulikemu, O. F. Mohammed, O. M. Bakr, Surface-Reconstructed InAs Colloidal Nanorod Quantum Dots for Efficient Deep-Shortwave Infrared Emission and Photodetection. *J. Am. Chem. Soc.* **2024**, 146, 29094–29103